J Therm Spray Tech (2018) 27:959–967
https://doi.org/10.1007/s11666-018-0733-z

PEER REVIEWED

Microstructure and Thermomechanical Properties of Atmospheric Plasma-Sprayed Yb_2O_3 Coating

Xin Zhong[1,2] · Yaran Niu[2] · Hong Li[1] · Xuebin Zheng[2] · Chuanxian Ding[2] · Jinliang Sun[1]

Submitted: 26 December 2017 / in revised form: 1 June 2018 / Published online: 19 June 2018

Abstract In this study, a Yb_2O_3 coating was fabricated by the atmospheric plasma spray technique. The phase composition, microstructure, and thermal stability of the coating were examined. The thermal conductivity and thermal expansion behavior were also investigated. Some of the mechanical properties (elastic modulus, hardness, fracture toughness, and flexural strength) were characterized. The results reveal that the Yb_2O_3 coating is predominantly composed of the cubic Yb_2O_3 phase, and it has a dense lamellar microstructure containing defects. No mass change and exothermic phenomena are observed in the thermogravimetry and differential thermal analysis curves. The high-temperature x-ray diffraction results indicate that no phase transformation occurs from room temperature to 1500 °C, revealing the good phase stability of the Yb_2O_3 coating. The coefficient of thermal expansion of the Yb_2O_3 coating is (7.50-8.67) $\times 10^{-6}$ K^{-1} in the range of 200-1400 °C. The thermal conductivity is about 1.5 W m^{-1} K^{-1} at 1200 °C. The Yb_2O_3 coating has excellent mechanical properties and good damage tolerant. The unique combination of these properties implies that the Yb_2O_3 coating might be a promising candidate for T/EBCs applications.

Keywords atmospheric plasma spray · environmental barrier coating · microstructure · thermal barrier coating · thermomechanical properties · Yb_2O_3 coating

✉ Yaran Niu
yrniu@mail.sic.ac.cn

Hong Li
lihong2007@shu.edu.cn

Xuebin Zheng
xbzheng@mail.sic.ac.cn

[1] Research Center of Composite Materials, Shanghai University, Shanghai 200072, China

[2] Key Laboratory of Inorganic Coating Materials CAS, Shanghai Institute of Ceramics, Chinese Academy of Sciences, Shanghai 200050, China

Introduction

Thermal barrier coatings (TBCs) are widely used in air- and land-based advanced gas turbines to improve the efficiency and extend the service life of the hot components (Ref 1, 2). Environmental barrier coatings (EBCs) have been developed to protect ceramic matrix composites (CMCs) from corrosion by water vapor (Ref 3-5). A number of studies have been focused on the thermomechanics and stability of T/EBC systems (Ref 6-13). TBC and EBC systems generally contain multilayer structures, such as bond and top layers. Among the multilayered structures, the top layer could be the most important for the performance of the designed coating system. Generally, the main properties that are needed for the top layer material are chemical and phase stability at high temperatures, relatively low thermal conductivity, a coefficient of thermal expansion (CTE) compatible with the substrate, and good mechanical properties (Ref 2, 5, 9).

Rare earth oxides (RE_2O_3, RE = rare earth elements) are used as raw materials to synthesize T/EBCs materials, such as rare earth silicates and zirconates, by solid-state reaction methods. Numerous rare earth silicates (RE_2SiO_5, RE = Y, Yb, Lu, Er, Gd, Tm, Dy, Tb, and $RE_2Si_2O_7$, RE = Y, Yb, Lu, Er) have been investigated, and the results indicate that these materials have relatively low thermal conductivity, good thermal stability, and good mechanical properties,

which means that they are promising candidates for T/EBCs applications (Ref 14-17). Moreover, pyrochlore-type rare earth zirconates ($RE_2Zr_2O_7$, RE = Yb, Y, Gd, Eu, Sm, Nd, La, Dy, and Er) have low thermal conductivity, excellent phase stability, and suitable CTE, indicating that they are promising TBC candidate materials (Ref 18). Besides Y_2O_3, some other rare earth oxides have been studied and applied to improve the phase stability or corrosion resistance, such as RE_2O_3 (RE = Sc, La, Nd, Sm, Gd, Dy, and Yb)-doped ZrO_2 counterparts (Ref 19).

It is speculated that rare earth oxides may be good high-temperature structural materials for T/EBCs applications. Mechnich et al. (Ref 20) deposited a Y_2O_3 coating on Al_2O_3/Al_2O_3 CMC as an EBC. Good adherence and remarkable stability of the Y_2O_3 coating were observed in the as-sprayed state as well as upon isothermal treatment up to 1400 °C. Moreover, thermal cyclic testing of the Y_2O_3 coating performed at 1200 °C revealed excellent durability. Golden et al. (Ref 21) investigated the volatility of Y_2O_3, SiO_2, and TiO_2 in a simulated turbine engine environment (1 atm H_2O pressure, 165-177 m s^{-1} steam-jet velocities, and 1240-1300 °C). They found that the oxide were in the forms of $Y(OH)_3$, $Si(OH)_4$, and $TiO(OH)_2$. The measured recession rate of Y_2O_3 ($\leq$ 0.01 μm h^{-1}) was significantly lower than those of SiO_2 (4.1 μm h^{-1}) and TiO_2 (0.92 μm h^{-1}), indicating that Y_2O_3 possesses excellent stability in water–vapor containing environment. Courcot et al. (Ref 22) studied the stability of RE_2O_3 (RE = Sc, Dy, Er, Yb) through volatilization tests at 1000-1400 °C temperatures in moist air with a gas velocity of 5 cm s^{-1}. They found that lanthanide oxides appear to be more stable than Y_2O_3 or Sc_2O_3. Yb_2O_3 appears to be the most stable rare earth oxide, because the partial pressures of $Yb(OH)_3$ and YbOOH are the lowest. The plasma spray technique has been widely used to fabricate protective coatings because of its high efficiency, capability of handling different substrates, and ability to generate relatively dense and uniform microstructures. The atmospheric plasma spray (APS) technique is a suitable method for preparation of T/EBCs. Thus, it is important to investigate the microstructure, thermal properties, and mechanical properties of rare earth oxide coatings fabricated by the APS technique.

In this study, we successfully prepared a Yb_2O_3 coating by the APS process. The phase composition and microstructure of the as-sprayed coating were characterized, and the thermal stability was investigated. Some of the thermal properties (thermal conductivity and thermal expansion behavior) and mechanical properties (elastic modulus, hardness, fracture toughness, and flexural strength) of the coating were investigated. This study might shed some light on the understanding of rare earth oxide coatings and their potential applications as T/EBCs materials.

Experimental Procedure

Sample Preparation

Commercial Yb_2O_3 powder (Shanghai Heli Rare Earth Material Co., Ltd., Shanghai, China) was used to prepare the Yb_2O_3 coating. The powder was ball-milled for 5 h using zirconia balls together with deionized water in a polyethylene bottle. After mixing, the suspension was sprayed in a drying tower [SFL-12, Okawara Powder Equipment (Shanghai) Co., Ltd., Shanghai, China] to produce a feedstock powder with spherical or near-spherical shapes. The obtained free-flowing powder is suitable for plasma spraying. The Yb_2O_3 coating was fabricated by a plasma spray system (A-2000, Sulzer Metco AG, Switzerland) equipped with a F4-MB torch. The operating spray parameters are listed in Table 1. The free-standing Yb_2O_3 coating (about 2 mm thick) was deposited on an aluminum substrate (128 mm × 84 mm × 2 mm) with a water-cooling system and then mechanically removed from the substrate for microstructure and thermomechanical property tests.

Specimen Characterization

The phase compositions of the powder and the as-sprayed coating were analyzed by x-ray diffraction (XRD, RAX-10, Rigaku, Japan) with Cu *Ka* (λ = 1.54056 Å) radiation. The particle size measurements were performed with a laser diffraction system (BT-9300Z, Bettersize Instruments Ltd., China). High-temperature XRD (HT-XRD, D8 ADVANCE, Bruker, Germany) was performed to investigate the phase stability of the coating. Data were recorded at 1300, 1400, and 1500 °C from 10° to 70° (2θ, step size 0.05°). The heating rate of the sample was 20 °C min^{-1} until the required temperature was reached, and this temperature was maintained for 15 min before the test. The microstructures of the powder and as-sprayed coating were characterized by scanning electron microscopy systems

Table 1 Operating parameters used for plasma spray

Parameters	Unit	Value
Power	kW	43
Primary plasma gas Ar	L min^{-1}	38
Secondary plasma gas H_2	L min^{-1}	12
Carrier gas Ar	L min^{-1}	3
Spray distance	mm	120

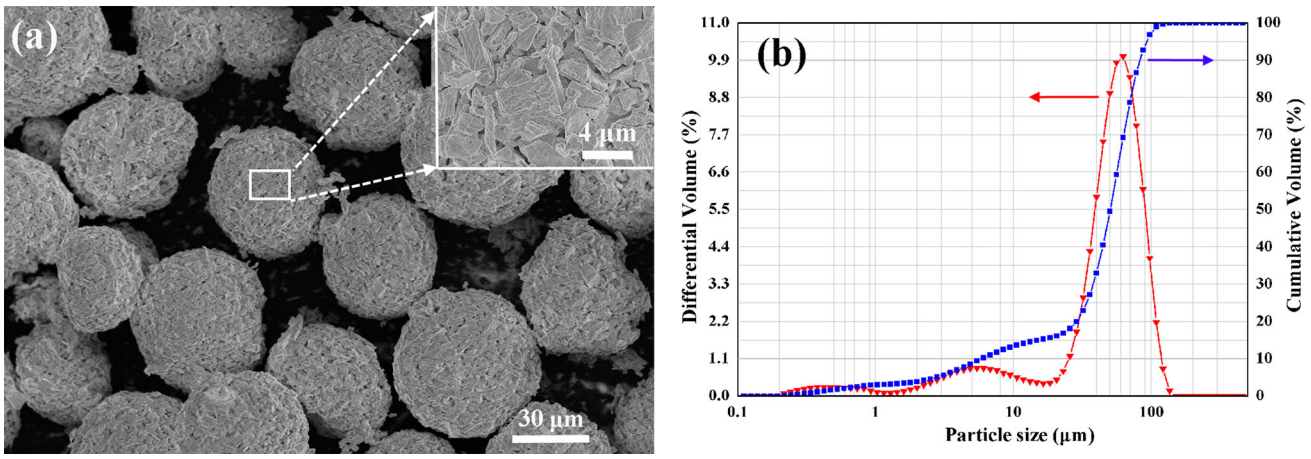

Fig. 1 Morphology (a) and particle size distribution (b) of Yb_2O_3 powder

(SEM, S-4800, Hitachi, Japan, and Magellan 400, FEI, USA).

The bulk density measurements were taken by the Archimedes method using distilled water as the medium. The coating porosity was evaluated by image analysis software. Five to eight back-scattered electron SEM (BSE-SEM) images with 1000× magnification of the cross section were randomly taken for each specimen for image analysis. The Vickers hardness (H_v) measurements were taken by Vickers indentation (Wilson-Wolpert Tukon 2100 B, Instron, USA) at a load of 1000 g with a dwell time of 15 s. The elastic modulus (E) was determined by a G-200 nanoindenter (Agilent Technologies, Oak Ridge, USA) equipped with a Berkovich indenter. The reported H_v and E data are the average values of ten indents, which were tested at different sites on the polished cross section of the coating. The fracture toughness (K_{IC}) was estimated based on the microhardness measurements by Eq 1:

$$K_{IC} = 0.16 H_v (c/a)^{-3/2} a^{1/2} \quad \text{(Eq 1)}$$

where $2a$ is the length of the indent diagonal and $2c$ is the combined length of the indent diagonal and crack. The flexural strength (σ) was determined by the three-point bending method, and six rectangular bulk samples with dimensions of 3.0 mm × 4.0 mm × 36.0 mm were measured to obtain the average value.

Simultaneous thermogravimetric and differential thermal analysis (TG–DTA, STA449C, Netzsch, Germany) were performed to investigate the thermal stability of the coating from room temperature to 1400 °C with a heating rate of 10 °C min^{-1}. The thermal expansion of the coating was determined by measuring the temperature-dependent changes of the sample lengths using a high-temperature dilatometer (TMA403F3, Netzsch, Germany). The laser flash method was performed to measure the thermal diffusivity (α) of the coating from 200 to 1200 °C at intervals of 100 °C. Before testing, the disk specimen with a size of 11.0 mm (diameter) × 0.8 mm (width) was coated with a thin graphite layer to prevent the laser beam from directly transmitting through the sample. The heat capacity (C_p) data of Yb_2O_3 were based on the Ref 23. The thermal conductivity (κ) values were calculated by

$$\kappa = C_p \times \alpha \times \rho \quad \text{(Eq 2)}$$

where ρ is the density.

Results and Discussion

Microstructure Characterization

The morphology and particle size distribution of the Yb_2O_3 powder are shown in Fig. 1. The spray-dried Yb_2O_3 powder is spherical or near-spherical (Fig. 1a). The particulates of the powder are composed of numerous small particles with irregular shapes and sizes of several micrometers, as shown in the high-magnification inset of Fig. 1(a). The measured medium size (D_{50}) of the powder is about 45 μm. The XRD patterns of the spray-dried Yb_2O_3 powder and Yb_2O_3 coating are shown in Fig. 2. The phase of the Yb_2O_3 coating is the same as that of the feedstock powder, which is composed of cubic Yb_2O_3 (c-Yb_2O_3). Clearly, the Yb_2O_3 powder exhibits excellent phase stability during the APS process.

Observation of the coating surface shows that the Yb_2O_3 coating mainly consists of completely melted deposits (Fig. 3a). Some microcracks are also observed, which was resulted from the release of thermal stresses during cooling (Fig. 3b). It is worth noting that grains with sizes about several nanometers form on the coating surface, as observed in the high-magnification image (Fig. 3c). The measured density of the Yb_2O_3 coating is about

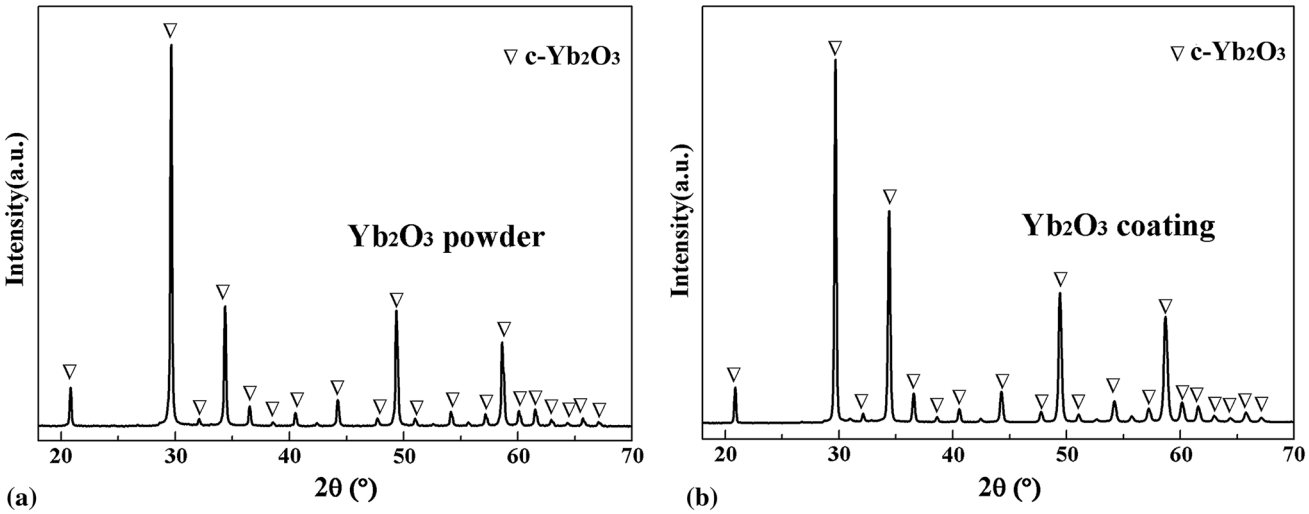

Fig. 2 XRD patterns of Yb_2O_3 powder (a) and as-sprayed Yb_2O_3 coating (b)

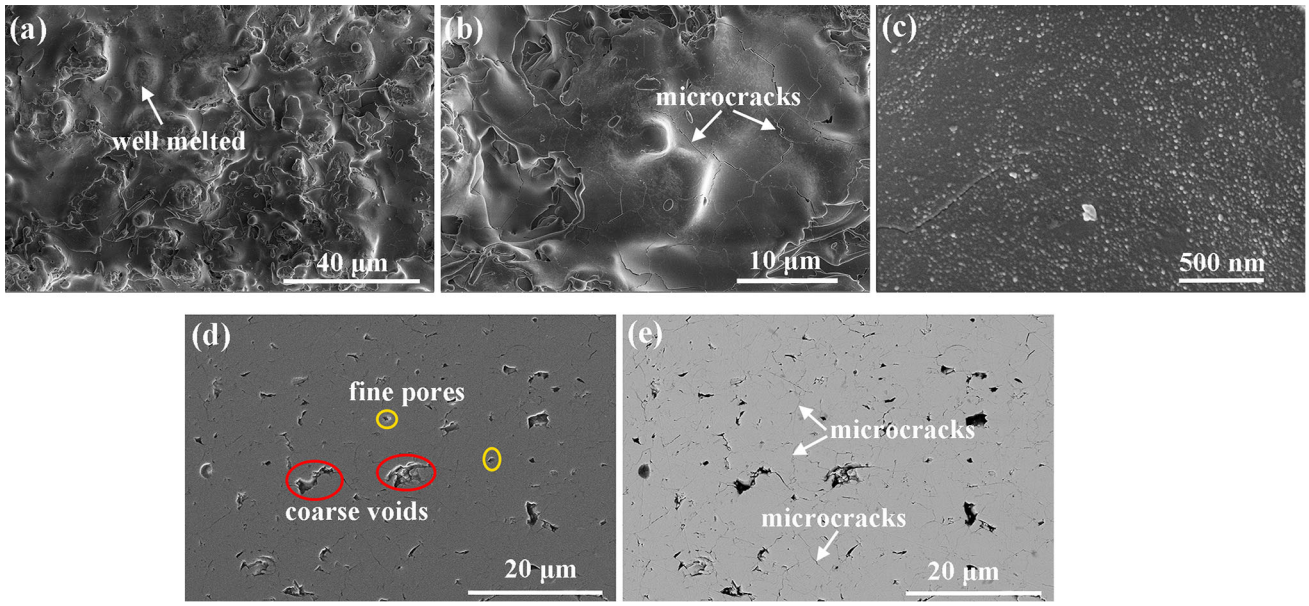

Fig. 3 Low (a) and high (b, c) magnification of surface morphologies and SE-SEM (d) and BSE-SEM (e) morphologies of cross section of Yb_2O_3 coating

8.40 g cm^{-3}. Figure 3(d) and (e) displays the scattered electron (SE)-SEM and BSE-SEM micrographs of the cross section of the Yb_2O_3 coating, respectively. The coating is relatively dense with low porosity of about 4.3%. Different types of defects exist in the coating, such as microcracks, fine pores (indicated by yellow circles in Fig. 3d), and coarse voids (indicated by red circles in Fig. 3d).

The fractural morphology of the Yb_2O_3 coating is shown in Fig. 4. It shows that the Yb_2O_3 coating has the typical laminar structure of plasma-sprayed coatings, which is mainly composed of splats overlapped layer by layer. Defects, such as interfaces, microcracks, and pores, are observed within the coating. The presence of microcracks could be related to shrinkage of the droplets and the release of accumulated thermal stresses during cooling. Collision of high-speed incoming semi-melted or un-melted particles with the earlier deposited layers might also result in formation of microcracks, although this requires further evidence. Besides microcracks, there are two typical types of pores in the Yb_2O_3 coating: fine pores and coarse voids. Fine pores within the splats might result from entrapped gas that does not have sufficient time to escape because of the rapid deposition of melted particles. The coarse voids located along the splat boundaries occur because of random overlap of splats. The high-magnification view (Fig. 4b)

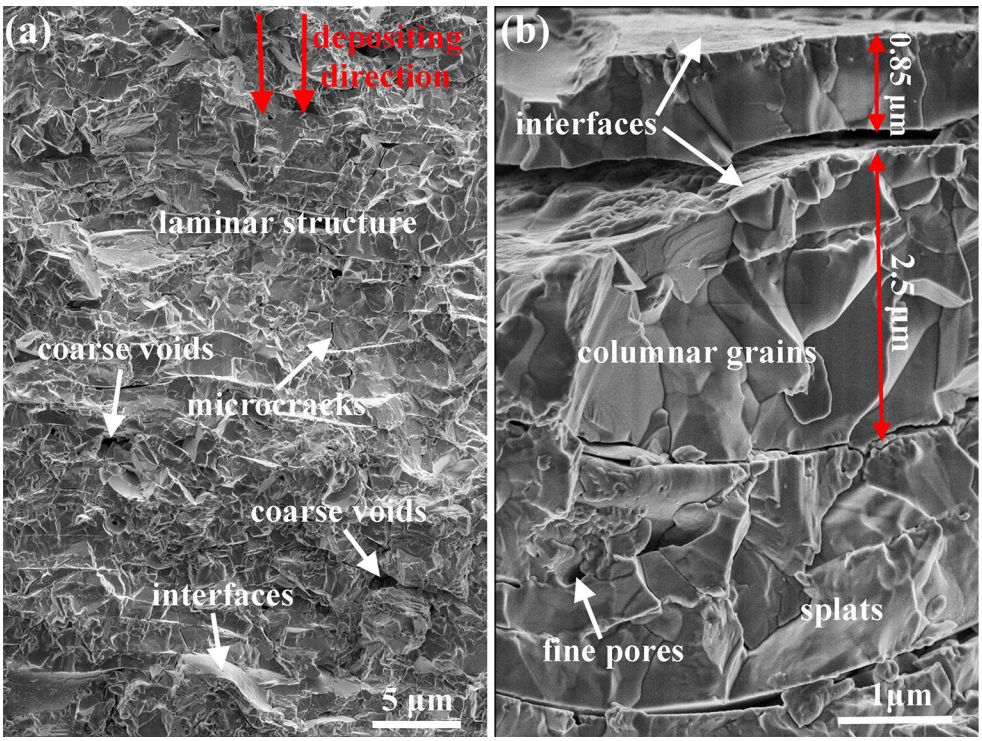

Fig. 4 Low (a)- and high (b)-magnification fracture section morphologies of Yb_2O_3 coating

gives more detailed microstructure information. The thicknesses of the individual splats are about 0.85-2.5 μm. Moreover, columnar grains are observed in the layered splats. Special structures, such as interfaces and pores, along the splat boundaries are conducive to reduction of the thermal conductivity of the Yb_2O_3 coating.

Property Characterizations

Thermal Stability

The HT-XRD patterns of the as-sprayed Yb_2O_3 coating at 1300, 1400, and 1500 °C are recorded and illustrated in Fig. 5. Comparing Fig. 2 with Fig. 5, the diffraction peaks of the as-sprayed Yb_2O_3 coating are almost the same as those of the coating exposed to high temperature. This confirms that no new phase is generated and no phase transformation occurs up to 1500 °C, indicating the good phase stability of the Yb_2O_3 coating.

The TG and DTA curves of the Yb_2O_3 coating are shown in Fig. 6. There is almost no mass change in the TG curve in the range from room temperature to 1200 °C, whereas there is a broad peak between 900 and 1200 °C in the DTA curve, which has two possible origins (Ref 24). On the one hand, it may be the relaxation region that is a feature of amorphous phase structures. On the other hand, wide peaks are observed from almost completely

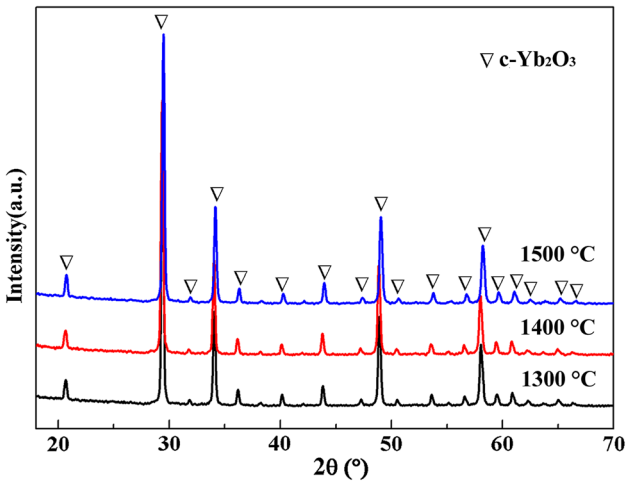

Fig. 5 HT-XRD patterns of Yb_2O_3 coating at different temperatures

crystalline materials, which may result from reduction of the residual stresses in the coating. Because the as-sprayed Yb_2O_3 coating consists of the crystalline c-Yb_2O_3 phase, the presence of a wide peak in the DTA curve can be attributed to the latter. Combining the HT-XRD and TG–DTA results, it can be concluded that the Yb_2O_3 coating has excellent thermal stability.

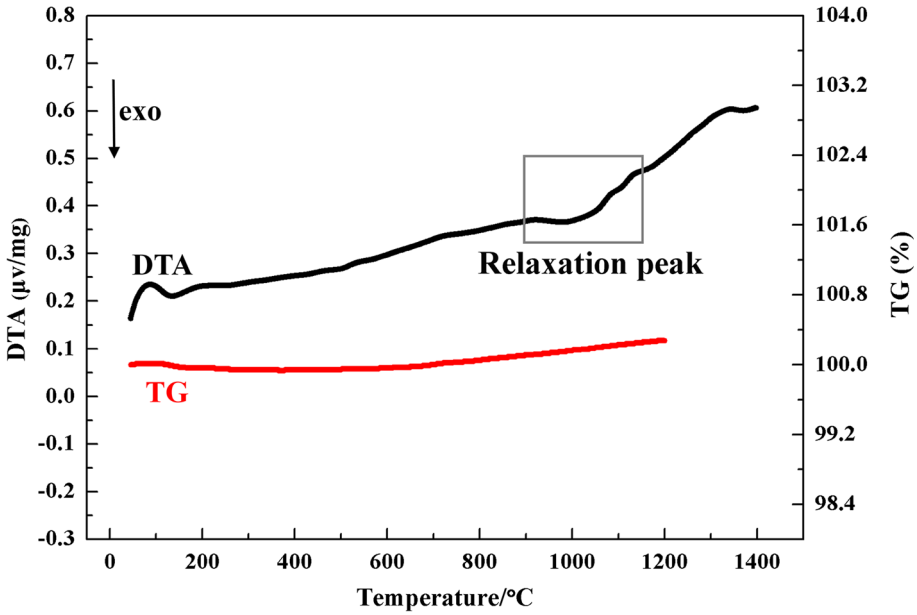

Fig. 6 TG-DTA curves of Yb_2O_3 coating

Thermal Properties

Generally, thermal expansion mismatch between the top layer and the bond layer, as well as the substrate, causes thermal stresses, which are the main cause of spallation failure of T/EBC systems during thermal cycling. Therefore, the thermal expansion behavior of the Yb_2O_3 coating was investigated, and the results are shown in Fig. 7. The $\Delta L/L$ curve is approximately linear from 200 to 1400 °C, demonstrating continuous volume expansion of the coating. The coefficient of thermal expansion (CTE) curve was obtained according to the slope of the thermal expansion rate versus the temperature during heating. In the range of 200-1400 °C, the CTE of the Yb_2O_3 coating is in the range of 7.50-8.67 $\times$ 10^{-6} K^{-1}, which is close to the range for Yb_2SiO_5 (7.00-8.00 $\times$ 10^{-6} K^{-1}) (Ref 25, 26).

Figure 8 illustrates the measured thermal diffusivity and calculated thermal conductivity of the Yb_2O_3 coating. It is clear that both curves decrease with increasing temperature up to 800 °C and then increase with further increasing temperature. The decrease in the thermal conductivity can be interpreted by the phonon conduction behavior (Ref 27). Phonons are scattered by grain boundaries and defects, and scattering is strengthened with increasing temperature, resulting in the thermal conductivity being inversely proportional to the temperature. The increase in the thermal conductivity can be attributed to microstructure changes, such as grain growth, microcrack healing, and pore shrinkage, because of the occurrence of sintering phenomena at temperatures above 800 °C. The thermal conductivity of the Yb_2O_3 coating is about 1.5 W m^{-1} K^{-1} at 1200 °C. This indicates that the conductivity of the Yb_2O_3 coating is close to those of some currently used T/EBC materials, such as YSZ and $Yb_2Si_2O_7$ (Ref 28).

Mechanical Properties

The durability of T/EBCs materials depends on the tolerance of the materials to exterior mechanical damage, which is related to their mechanical properties. Therefore, the mechanical properties of the Yb_2O_3 coating need to be determined to its potential applications as T/EBCs materials. The measured mechanical properties of the Yb_2O_3 coating are given in Table 2, along with the values of some T/EBCs materials for comparison. The elastic modulus of the Yb_2O_3 coating is 100.8 $\pm$ 5.5 GPa, which is close to the value of the as-sprayed Yb_2SiO_5 coating of 97.3 $\pm$ 3.1 GPa. Compared with the bulk materials, the elastic moduli of the corresponding thermal sprayed materials are known to be much lower, which is closely related to their unique microstructure and inhomogeneity, such as the pore morphology and lamellar structure. Leigh et al. (Ref 31) reported that the elastic moduli of thermal spray materials are 12-78% of those of the bulk materials, depending on the materials, spray processes, and post-treatments. For T/EBCs materials, a low elastic moduli is favorable for reduction of the thermal stresses, which endows the Yb_2O_3 coating with good resistance to thermal shock (Ref 32). The measured H_v value of the Yb_2O_3 coating is 3.9 $\pm$ 0.1 GPa, which is lower than that of the Yb_2SiO_5 coating of 5.1 $\pm$ 0.1 GPa. The low Vickers hardness might be caused by the weak bonding between Yb and O atoms in the crystal structure.

Several quantitative measures can be used to describe the damage tolerance of ceramic materials. Boccaccini

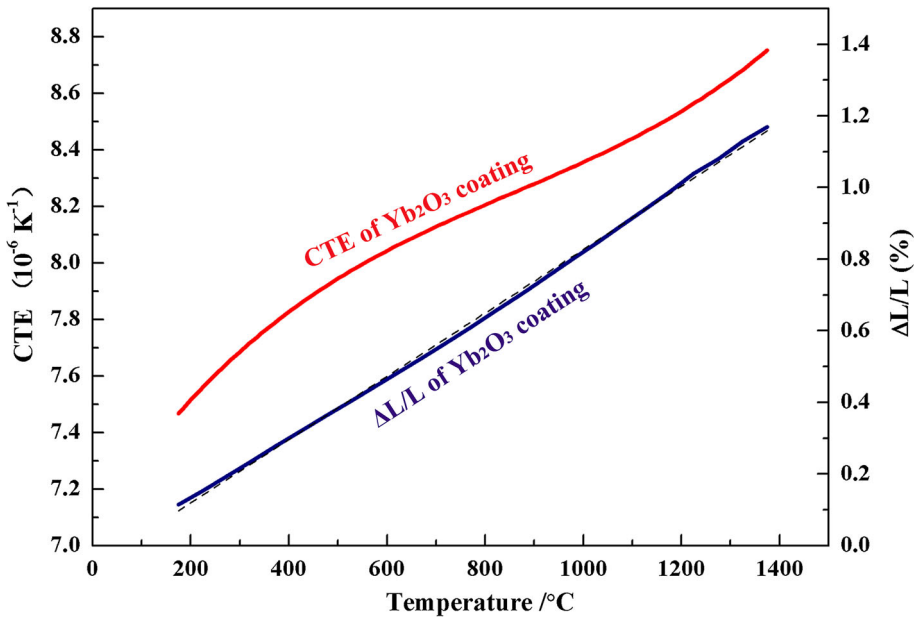

Fig. 7 Thermal expansion behavior of Yb_2O_3 coating

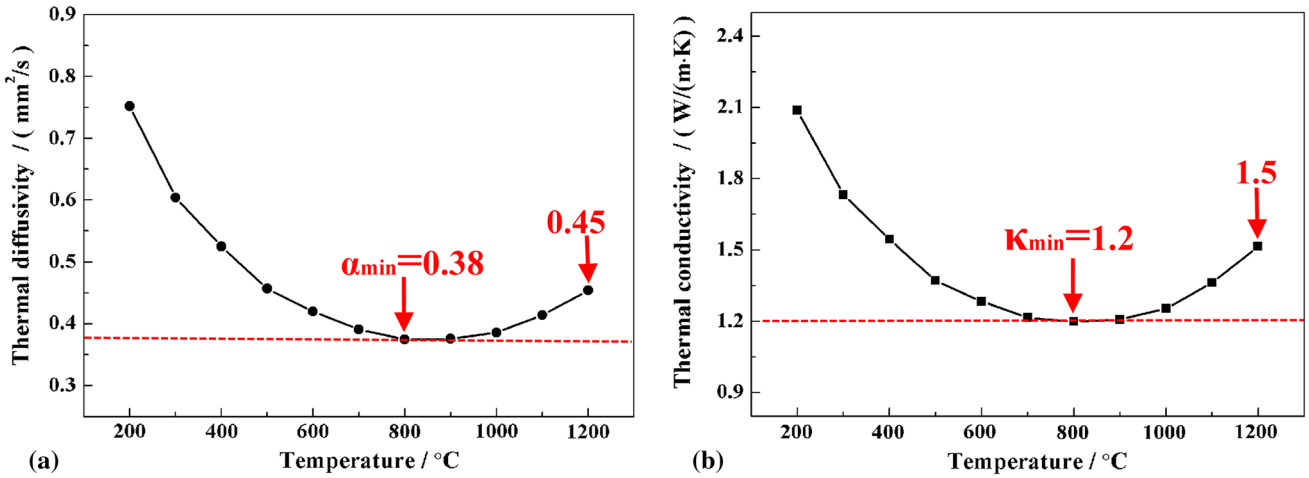

Fig. 8 Thermal diffusivity (a) and thermal conductivity (b) vs. temperature of Yb_2O_3 coating

et al. (Ref 33) used the brittleness index M to distinguish brittle and ductile materials:

$$M = H_v/K_{IC} \quad \text{(Eq 3)}$$

A low M value indicates good damage tolerance. According to the data in Table 2, the Yb_2O_3 coating has a lower M value (2.15 $\mu m^{1/2}$) than those of the T/EBCs materials, such as Yb_2SiO_5 (2.78 $\mu m^{1/2}$), $Yb_2Si_2O_7$ (3.40 $\mu m^{1/2}$), and $Yb_3Al_5O_{12}$ (3.70 $\mu m^{1/2}$). Bao et al. (Ref 34) proposed D_t as a quantitative measurement of the damage tolerance:

$$D_t = \frac{K_{IC} \cdot E}{\sigma \cdot H_v} \quad \text{(Eq 4)}$$

A high D_t value means good damage tolerance. According to the data in Table 2, the D_t value of the Yb_2O_3 coating was calculated to be 0.43 $m^{1/2}$, which is higher than those of some reported T/EBCs materials, such as Yb_2SiO_5 (0.25 $m^{1/2}$) and $Yb_2Si_2O_7$ (0.38 $m^{1/2}$). Moreover, the D_t value of the Yb_2O_3 coating is the same as that of $Yb_3Al_5O_{12}$ (0.43 $m^{1/2}$), while it is slightly lower than that of Y_2SiO_5 (0.51 $m^{1/2}$). The above results show that the Yb_2O_3 coating may have excellent mechanical properties and good damage tolerance, which are propitious for its applications as T/EBCs materials.

Conclusions

A Yb_2O_3 coating has been fabricated by the APS technique. The microstructure, thermal properties, and mechanical properties of the Yb_2O_3 coating were

Table 2 Comparison of mechanical properties of Yb_2O_3 coating with those of T/EBCs materials

Materials	Preparation method	Hardness H_v, GPa	Elastic modulus E, GPa	Fracture toughness K_{IC}, MPa $m^{1/2}$	Flexure strength σ, MPa	M	D_t
Yb_2O_3 coating	A	3.9 ± 0.1(a)	100.8 ± 5.5	1.81 ± 0.07	107 ± 7	2.15	0.43
Yb_2SiO_5 coating (Ref 26)	A	5.1 ± 0.1(a)	97.3 ± 3.1	…	…	…	…
Bulk Yb_2SiO_5 (Ref 14)	B	6.4 ± 0.1(a)	149	2.3 ± 0.1	215 ± 12	2.78	0.25
Bulk $Yb_2Si_2O_7$ (Ref 15)	C	6.8 ± 0.2(a)	171	2.0 ± 0.1	137 ± 7	3.40	0.38
Bulk Y_2SiO_5 (Ref 16)	B	5.3(a)	123	2.2	100	2.41	0.51
Bulk $Y_2Si_2O_7$ (Ref 17)	B	6.2 ± 0.1(a)	155	2.12 ± 0.05	135 ± 4	2.92	0.39
Bulk $Yb_3Al_5O_{12}$ (Ref 29)	C	10.7 ± 0.4(a)	282	2.88 ± 0.14	176 ± 5	3.70	0.43
8YSZ coating	A	3.36 ± 0.45(b) (Ref 30)	25 (Ref 30)	1.08 ± 0.06 (Ref 30)	33 ± 7 (Ref 30)	…	…
		3.4(b) (Ref 31)	44 ± 6 (Ref 31)				

A APS
B Isostatically cold pressing + pressure-less sintering
C Isostatically cold pressing + hot pressing sintering
(a) Vickers hardness. (b) Knoop hardness

investigated. Microstructure observation shows that the coating is composed of a dense laminar structure. The Yb_2O_3 coating is the c-Yb_2O_3 phase, and it shows outstanding phase stability at high temperature. In the range 200-1400 °C, the CTE of the Yb_2O_3 coating is in the range of 7.50-8.67 × 10^{-6} K^{-1}. The thermal conductivity is about 1.5 W m^{-1} K^{-1} at 1200 °C. Mechanical property tests reveal that the Yb_2O_3 coating has a low brittleness index and high D_t value, showing that the Yb_2O_3 coating may belong to damage tolerant materials. The dense microstructure, suitable CTE, low thermal conductivity, and high temperature stability combined with its excellent mechanical properties indicate that the Yb_2O_3 coating may have potential applications as T/EBCs materials.

Acknowledgments This work was supported by the Engineering case study in extreme conditions using system mechanics approach (XDB22010202) and the Youth Innovation Promotion Association of the Chinese Academy of Sciences (2014223).

References

1. R.A. Miller, Thermal Barrier Coatings for Aircraft Engines—History and Direction, *J. Therm. Spray Technol.*, 1997, **6**(1), p 35-42
2. X.Q. Cao, R. Vassen, and D. Stoever, Ceramic Materials for Thermal Barrier Coatings, *J. Eur. Ceram. Soc.*, 2004, **24**(1), p 1-10
3. S. Zhu, M. Mizuno, Y. Nagano, J. Cao, Y. Kagawa, and H. Kaya, Creep and Fatigue Behavior in An Enhanced SiC/SiC Composite at High Temperature, *J. Am. Ceram. Soc.*, 1998, **81**(9), p 2269-2277
4. N.S. Jacobson, Corrosion of Silicon-Based Ceramics in Combustion Environments, *J. Am. Ceram. Soc.*, 1993, **76**(1), p 3-28
5. K.N. Lee, Current Status of Environmental Barrier Coatings for Si-based Ceramics, *Surf. Coat. Technol.*, 2000, **133-134**, p 1-7
6. É. Darthout and F. Gitzhofer, Thermal Cycling and High-Temperature Corrosion Tests of Rare Earth Silicate Environmental Barrier Coatings, *J. Therm. Spray Technol.*, 2017, **26**(8), p 1823-1837
7. B.J. Harder, J. Ramírez-Rico, J.D. Almer, K.N. Lee, and K.T. Faber, Chemical and Mechanical Consequences of Environmental Barrier Coating Exposure to Calcium-Magnesium-Aluminosilicate, *J. Am. Ceram. Soc.*, 2011, **94**(S1), p S178-S185
8. D.L. Poerschke, D.D. Hass, S. Eustis, G.G.E. Seward, J.S.V. Sluytman, and C.G. Levi, Stability and CMAS Resistance of Ytterbium-Silicate/Hafnate EBCs/TBC for SiC Composites, *J. Am. Ceram. Soc.*, 2015, **98**(1), p 278-286
9. D.L. Poerschke, R.W. Jackson, and C.G. Levi, Silicate Deposit Degradation of Engineered Coatings in Gas Turbines: Progress Toward Models and Materials Solutions, *Annu. Rev. Mater. Res.*, 2017, **47**, p 297-330
10. D.L. Poerschke, J.S. Van Sluytman, K.B. Wong, and C.G. Levi, Thermochemical Compatibility of Ytterbia-(Hafnia/Silica) Multilayers for Environmental Barrier Coatings, *Acta Mater.*, 2013, **61**(18), p 6743-6755
11. B.T. Richards, S. Sehr, F. de Franqueville, and H.N.G. Wadley, Fracture Mechanisms of Ytterbium Monosilicate Environmental Barrier Coatings During Cyclic Thermal Exposure, *Acta Mater.*, 2016, **103**, p 448-460

12. B.T. Richards, M.R. Begley, and H.N.G. Wadley, Mechanisms of Ytterbium Monosilicate/Mullite/Silicon Coating Failure During Thermal Cycling in Water Vapor, *J. Am. Ceram. Soc.*, 2015, **98**(12), p 4066-4075
13. B.T. Richards, K.A. Young, F.D. Francqueville, S. Sehr, M.R. Begley, and H.N.G. Wadley, Response of Ytterbium Disilicate-Silicon Environmental Barrier Coatings to Thermal Cycling in Water Vapor, *Acta Mater.*, 2016, **106**, p 1-14
14. M.H. Lu, H.M. Xiang, Z.H. Feng, X.Y. Wang, and Y.C. Zhou, Mechanical and Thermal Properties of Yb_2SiO_5: A promising Material for T/EBCs Applications, *J. Am. Ceram. Soc.*, 2016, **99**(4), p 1404-1411
15. Z.L. Tian, L.Y. Zheng, J.M. Wang, and J.B. Yang, Damage Tolerance and Extensive Plastic Deformation of β-$Yb_2Si_2O_7$ From Room to High Temperatures, *J. Am. Ceram. Soc.*, 2015, **98**(9), p 2843-2851
16. Z.Q. Sun, Y.C. Zhou, J.Y. Wang, and M.S. Li, Mechanical Properties and Damage Tolerance of Y_2SiO_5, *J. Eur. Ceram. Soc.*, 2008, **28**(15), p 2895-2901
17. Z.Q. Sun, Y.C. Zhou, J.Y. Wang, and M.S. Li, Γ-$Y_2Si_2O_7$, A Machinable Silicate Ceramic: Mechanical Properties and Machinability, *J. Am. Ceram. Soc.*, 2007, **90**(8), p 2535-2541
18. H. Yamamura, H. Nishino, and K. Kakinuma, Relationship Between Oxide-Ion Conductivity and Dielectric Relaxation in the $Ln_2Zr_2O_7$ System Having Pyrochore-Type Compositions (Ln = Yb, Y, Gd, Eu, Sm, Nd, La), *J. Phys. Chem. Solids*, 2008, **69**(7), p 1711-1717
19. R.L. Jones, Some Aspects of the Hot Corrosion of Thermal Barrier Coatings, *J. Therm. Spray Technol.*, 1997, **6**(1), p 77-84
20. P. Mechnich and W. Braue, Air Plasma-Sprayed Y_2O_3 Coatings for Al_2O_3/Al_2O_3 Ceramic Matrix Composites, *J. Eur. Ceram. Soc.*, 2013, **33**(13-14), p 2645-2653
21. R.A. Golden and E.J. Opila, A Method for Assessing the Volatility of Oxides in High-Temperature High-Velocity Water Vapor, *J. Eur. Ceram. Soc.*, 2016, **36**(5), p 1135-1147
22. E. Courcot, F. Rebillat, F. Teyssandier, and C. Louchet-Pouillerie, Stability of Rare Earth Oxides in a Moist Environment at Elevated Temperatures-Experimental and Thermodynamic Studies Part II: Comparison of the Rare Earth Oxides, *J. Eur. Ceram. Soc.*, 2010, **30**(9), p 1911-1917
23. D.L. Ye, *Inorganic Material Thermodynamics*, 2nd ed., Metallurgical Industry Press, Beijing, 2002, p 1161-1162
24. F. Tarasi, M. Medraj, A. Dolatabadi, J. Oberste-Berghaus, and C. Moreau, Phase Formation and Transformation in Alumina/YSZ Nanocomposite Coating Deposited by Suspension Plasma Spray Process, *J. Therm. Spray Technol.*, 2010, **19**(4), p 787-795
25. DOE-National Energy Technology Laboratory, Protective Coatings for Gas Turbines. http://www.netl.doe.gov/File%20Library/Research/Coal/energy%20systems/turbines/handbook/4-4-2.pdf/, 2005. Accessed 12.06.11.
26. X. Zhong, Y.R. Niu, H. Li, Y. Zeng, X.B. Zheng, C.X. Ding, and J.L. Sun, Microstructure Evolution and Thermomechanical Properties of Plasma-Sprayed Yb_2SiO_5 Coating During Thermal Aging, *J. Am. Ceram. Soc.*, 2017, **100**(5), p 1896-1906
27. G.E. Youngblood, R.W. Rice, and R.P. Ingel, Thermal Diffusivity of Partially and Fully Stabilized (Yttria) Zirconia Single Crystals, *J. Am. Ceram. Soc.*, 1988, **71**(4), p 255-260
28. D.R. Clarke and S.R. Phillpot, Thermal Barrier Coating Materials, *Mater. Today*, 2005, **8**(6), p 22-29
29. X.F. Wang, H.M. Xiang, X. Sun, J.C. Liu, F. Hou, and Y.H. Zhou, Mechanical Properties and Damage Tolerance of Bulk $Yb_3Al_5O_{12}$ Ceramic, *J. Mater. Sci. Technol.*, 2015, **31**(4), p 369-374
30. S.R. Choi, D.M. Zhu, and R.A. Miller, Mechanical Properties/Database of Plasma-Sprayed ZrO_2-8wt% Y_2O_3 Thermal Barrier Coatings, *Int. J. Appl. Ceram. Technol.*, 2004, **1**(4), p 330-342
31. S.H. Leigh, C.K. Lin, and C.C. Berndt, Elastic Response of Thermal Spray Deposits under Indentation Tests, *J. Am. Ceram. Soc.*, 1997, **80**(8), p 2093-2099
32. K.N. Lee, J.I. Eldridge, and R.C. Robinson, Residual Stresses and Their Effects on the Durability of Environmental Barrier Coatings for SiC Ceramics, *J. Am. Ceram. Soc.*, 2005, **88**(12), p 3483-3488
33. A.R. Boccaccini, Machinability and Brittleness of Glass-Ceramics, *J. Mater. Process. Technol.*, 1997, **65**(1-3), p 302-304
34. Y.W. Bao, C.F. Hu, and Y.C. Zhou, Damage Tolerance of Nanolayer-Grained Ceramic: A Quantitative Estimation, *Mater. Sci. Technol.*, 2006, **22**(2), p 227-230